Supporting Information:

The Q_o Site.

Oxidation of the ubiquinol substrate of the cyt bc_1 complex takes place in the Q_o site, lying between the two electron transport chains which start at the Rieske Fe_2S_2 cluster (high-potential chain) and the cyt b_L heme (low-potential chain). The volume of the Q_o site, as identified by software such as Q-Site Finder[2], is much larger than the substrate and it has long been known that Q_o can bind large inhibitors. The Q_o site is shown as a glass volume in Fig. S1 (from PDB: 3CX5) along with the two cyt *b* hemes and the Fe_2S_2 cluster for reference. Representatives (stigmatellin and MOA-stilbene) of the two major classes of inhibitors are shown in the Q_o site. Each of them is larger than the substrate yet they occupy only a portion of the site. There is clearly much more room than is needed by substrate and there are numerous suggestions of substrate movement within the Q_o site as part of the catalytic reaction. The two regions for the trapped SQ_o identified by our PRE measurements are shown in green and purple and help localize SQ_o to small and specific regions of the Q_o site.

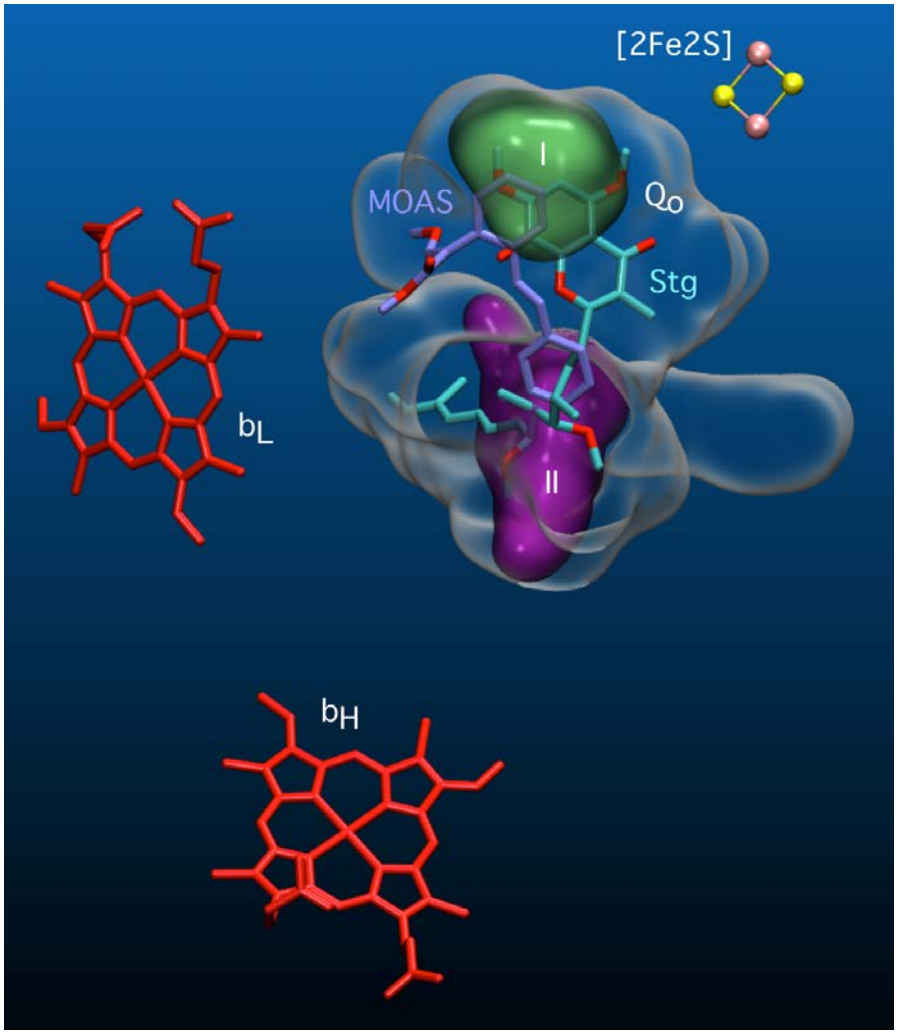

Figure S1. Volumetric representation of the yeast bc_1 Q_o site (Q_o void volume represented as a glass surface) showing location of SQ niches I and II as described in the text and bound stigmatellin (cyan, Stg) and MOA-stilbene (lilac, MOAS), representative b_L-distal and b_L-proximal inhibitors respectively[1]. The Q_o-docked Rieske Fe_2S_2 cluster is also shown and cytochrome *b* prosthetic groups b_L and b_H. This figure was prepared using PDB coordinates 3CX5[3].

Hyperfine Couplings.

The ENDOR simulations find two hyperfine tensors from two sets of protons. The simulations in Fig. 1C and 1D show the numbers of protons in the two sets are in a 3:1 ratio. This ratio immediately suggests that the two sets of protons are: a rapidly-rotating methyl group at the 5- position in ubiquinone with 3 protons; and one of the $–CH_2-$ protons on the hydrocarbon tail at the 4- position. If the tail is rotated out of plane with respect to the quinone ring, the two protons in the $–CH_2-$ group are magnetically inequivalent and their hyperfine couplings depend on the dihedral angle they make with the plane of the quinone ring, see, for example, the discussion of hyperconjugation in [13]. In frozen solutions of ubiquinone radical anions, the hydrocarbon tail is presumably frozen with a wide range of dihedral angles and hyperfine couplings and consequently does not produce distinct features in ENDOR or HYSCORE spectra, but in proteins such as the bacterial photosynthetic reaction center (bRC) it can have a single conformation with distinct spectral features. However, different protein binding sites force different conformations of the hydrocarbon tail. Considerable variation in the hyperfine couplings of the hydrocarbon tail can be expected in different proteins. On the other hand, the rapidly-rotating 5-methyl group has couplings reflecting the electronic structure of the radical, in particular the unpaired electron spin density around the quinone ring.

Table S1. Proton Hyperfine Tensors for SQ Radicals of Ubiquinone in Proteins and Frozen Solutions Determined by ENDOR or HYSCORE

System	Hyperfine Principal Values (MHz)	Reference
	Radical Anion $–CH_3$	
Q_o in Cyt *bc₁*	8.0, 4.0, 3.5	Present work
Q_A in bRCs	6.8, 3.6, 3.6	[4]
	7.1, 4.0, 4.0	[4b]
	6.68, 3.59, 3.09	[4a]
	6.9, 3.8, 3.2	[4a, 5]
	7.8, 2.7, 2.7	[6]
	7.2, 2.4, 2.4	[6]
Q_B in bRCs	7.9, 4.7, 4.7	[4b]
	7.8, 4.4, 3.9	[4a, 5, 7]
in *i*-propanol	8.5, 4.8, 4.8	[8]
in DME/MTHF	8.4, 5.2, 5.2	[9]
	Disputed neutral $–CH_3$	
Q_H in Cyt *bo₃*	13.4, 8.3, 8.3	[10]
	12.78, 8.40, 7.85	[11]
	Radical Anion $–CH_2–$	
Q_o in Cyt *bc₁*	11.5, 5.5, 5.0	Present work
Q_A in bRCs	8.8, 5.4, 5.4	[4]
	8.85, 5.51, 4.95	[4a]
	8.6, 5.6, 5.0	[12]
	H bonds	
Q_A in bRCs	8.8, -4.4, -5.7	[12]
	9.6, -6.8, -6.8	[6]
	10,-5.2, -5.2	[6]
Q_B in bRCs	9.6, -6.0, -6.0	[6]
	6.5,-4.6, -4.6	[6]
	4.9, -0.8,-0.8	[6]
	8.1,2.4, 2.4	[6]

The principal values of the hyperfine couplings from some well-characterized ubiquinone radicals are collected in Table S1. The couplings for the 5-methyl group of the radical anion both in bRCs and frozen solution are very similar to those measured here for the SQ_o. A reportedly more neutral ubiquinone radical in cyt *bo*$_3$ has distinctly larger 5-methyl couplings. There are fewer reported couplings for the hydrocarbon tail in the 4- position, as expected. Couplings for protons that form hydrogen bonds to the carbonyl oxygens are also listed and show large variation, but generally having small isotropic couplings.

The couplings fall into clear groups when the dipolar part of the hyperfine coupling is plotted against the isotropic hyperfine coupling, Fig. S2. The couplings are not always reported with consistent sign convention, so the perpendicular dipolar coupling is taken as half the magnitude of the largest magnitude component of the traceless hyperfine tensor and the isotropic value is one third of the trace.

All but one of the H-bonded protons (filled triangles) form a group with isotropic hyperfine couplings between ±2 MHz. The 5-methyl protons from established radical anions (filled dots) cluster in a group with isotropic value between 3-7 MHz, along with SQ_o (green square) and an H-bonded outlier. The 5-methyl coupling attributed to a neutral ubiquinone radical (red squares) form the last group with isotropic coupling larger than 8 MHz. Assignment of the two sets of protons from the ENDOR simulations as the 5-methyl group and the 4-position hydrocarbon tail of a ubiquinone radical anion agrees with reported hyperfine couplings and the relative numbers of nuclei.

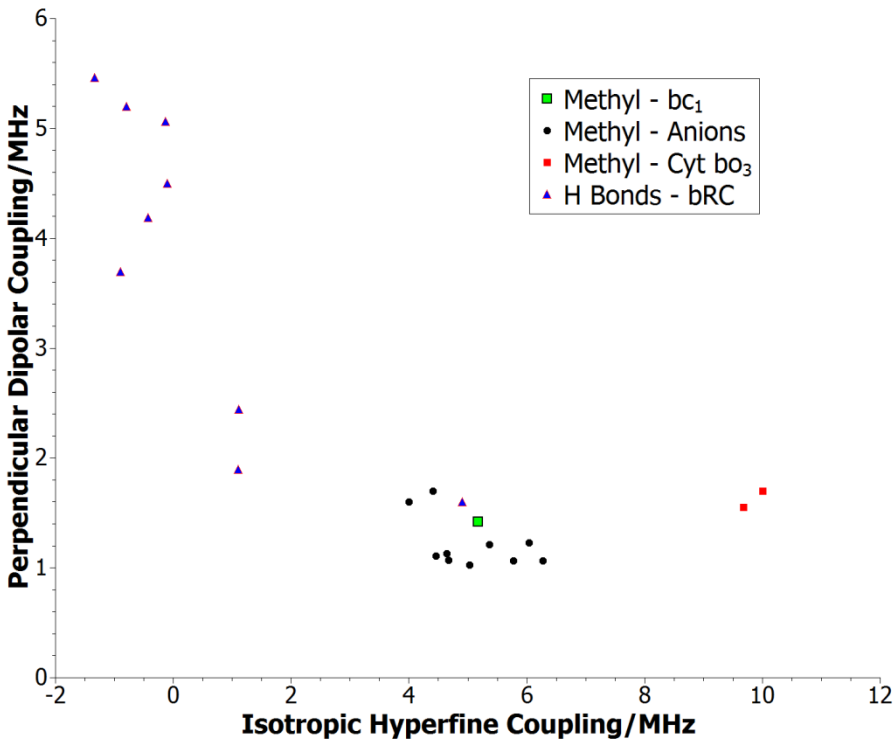

Figure S2. Plot of the dipolar coupling versus isotropic hyperfine coupling for protons of ubiquinone radicals in Table S1.

The EPR Spectrum.

The freeze quenched samples have a number of overlapping EPR signals. The largest amount of paramagnetic species is the 80 μM horse heart cyt *c* used to prevent full oxidation of the high-potential chain. Other paramagnetic centers are generated by the reaction of cyt bc_1: oxidized cyt *b* and c_1 and the reduced Rieske Fe_2S_2 cluster[14]. Each of these species have an EPR signal that overlaps that of the SQ_o, but linewidths, lineshapes and relaxation times differ by orders of magnitude so it is impossible to observe all of them in a single conventional cw- or pulsed EPR spectrum [14]. In addition, the pulsed EPR resonator was delivered with a significant background signal, resembling Cu(II), that overlaps the SQ_o spectrum.

It is possible to use EPR passage effects[15] to acquire an absorption-like EPR spectrum showing all of the species. Unfortunately the lineshapes and relative intensities of the different species can be severely distorted. A passage-effect spectrum, Fig. S3, measured at 7 K shows signals from all of the species in the freeze-quenched samples. The intense line near the center from SQ_o saturated the receiver and is clipped and slightly distorted. The broad features extending from ~2000 G to above 5500 G are the overlapping signals of the *b* and *c* hemes. Weaker features from the Rieske Fe_2S_2 cluster and the resonator background are indicated on the figure.

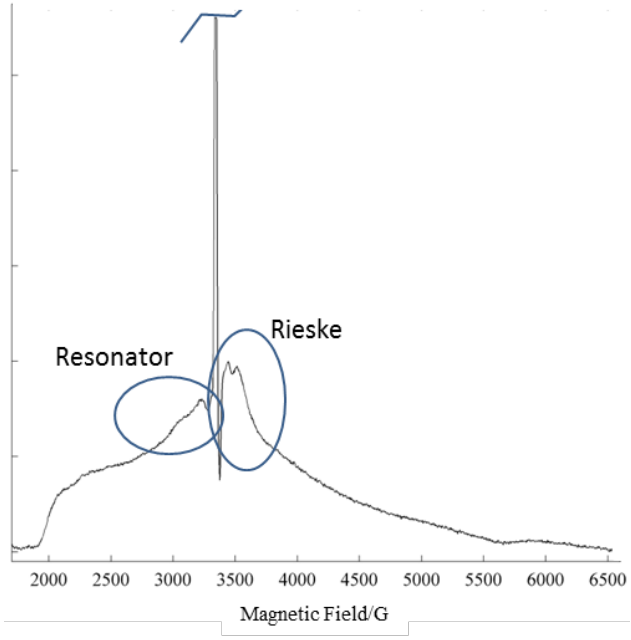

Figure S3. Absorption-like EPR spectrum measured using passage effects at 7 K with a freeze quenched sample of cyt bc_1. The spectrum was measured at 9.462 GHz using a microwave power of 0.21 mW and 20 G modulation at 100 KHz. The receiver was set to detect the second harmonic 90° out-of-phase with the modulation.

The background signals from sources other than SQ_o are broad and change slowly in the vicinity of the SQ_o signal. In particular, the decay of the two-pulse spin echo from the other signals had the same kinetics over that region. The decay measured just beyond the edge of the SQ_o signal was subtracted, after intensity correction, from decays at the center of the SQ_o signal. This correction produced the decays shown in Fig. 2 and used in the PRE fitting.

The Spin Echo Decay.

The electron spin echo decays by many routes [16], some depend primarily on the radical and others primarily on its environment. The different decay routes are mostly independent of each other, so the total decay is just the product of the decays from the individual routes. The decay of the spin echo of the radical anion of ubiquinone in cyclo-hexanol, Fig. 2, is rather slow with the echo lasting much longer

than 2 μs. This relatively slow decay sets a limit on the inherent decay rate of the radical anion and shows that the much more rapid decay of the SQ_o spin echo is caused by its protein environment. One important decay route is caused by nuclear spin diffusion or T_{2N} taking place in the protein more than half a nm from the radical [16b, 16c], which is temperature independent. Another route is the PRE, which is caused by dipolar interactions with rapidly-relaxing paramagnetic centers and does depend on temperature.

The PRE can be visualized qualitatively by looking at changes in the initial slopes of the decays of the spin echo (with the periodic modulation by proton ESEEM ignored)), even though the decays are not simple exponentials or stretched exponentials. The initial slope for the ubiquinone radical anion in cyclo-hexanol, Fig. S4, does not change until ~60 K where librational motion of the solvent and/or radical begins to affect the echo decay [17]. The SQ_o decay shows a prominent resonance-like peak at 35 K similar to peaks reported for PRE in other proteins [18], in addition to a large librational increase at high temperatures. Although this plot reveals the presence of PRE, a more detailed analysis of the data is required to determine distances to the centers responsible for this effect.

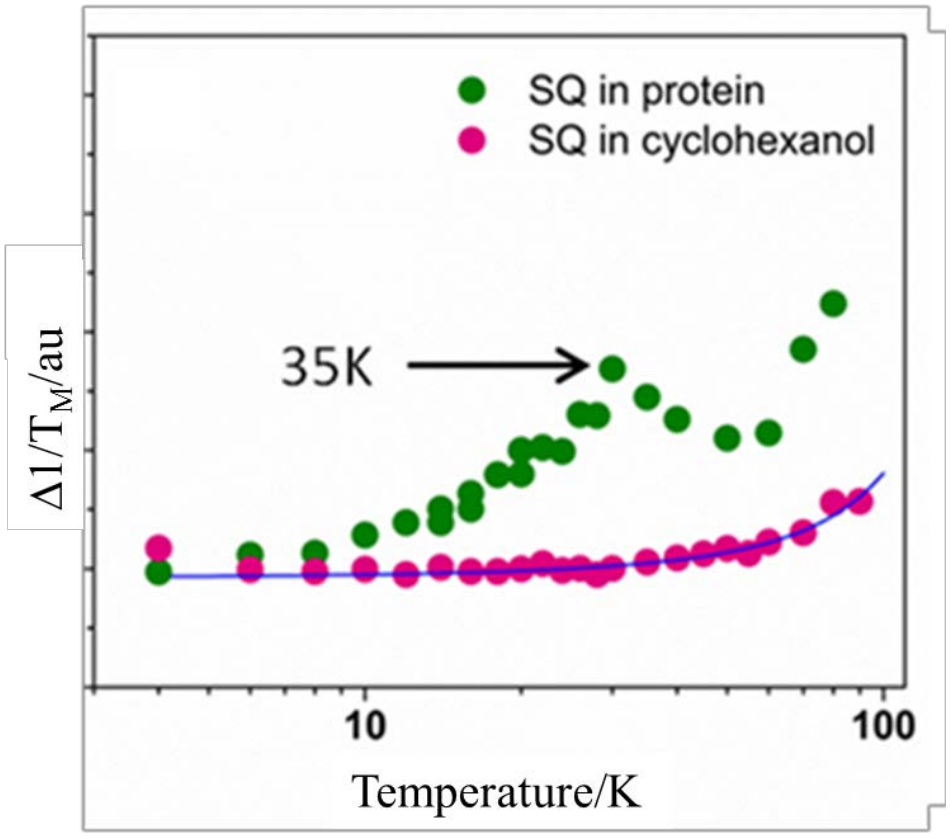

Figure S4. Plot of the change in initial slope of the spin echo decay versus temperature for the ubiquinone radical anion in cyclo-hexanol (magenta) and for SQ_o in mitochondrial cyt bc_1 (green).

Redox States of the Samples.

The SQ_o radical in these freeze-quenched samples exists in several distinct states of the protein. Freeze-quenching traps a mixture of the species present in the reaction mixture. In our samples with AA inhibiting the Q_i site, the first turnover in a monomer can be expected to send one electron down the high-potential chain to the Rieske Fe_2S_2 cluster and on to cyt c_1 and possibly soluble cyt *c* serving as a sacrificial electron acceptor. The second electron in the first turnover would rapidly enter the low-potential chain and reduce the b_H heme, leaving no SQ_o. In the second turnover, its first electron proceeds down the high-potential chain as before while the second electron either reduces the b_L heme, or remains on the substrate to produce SQ_o since their redox potentials are similar. If there is a third turnover, the first electron can enter the high-potential chain if at least one of the previous electrons to enter it has been passed on to soluble cyt *c*. The second electron on the third turnover cannot enter the filled low-potential chain and remains on SQ_o. After two or three turnovers, this very simplified outline shows the SQ_o in a monomer that may or may not have the b_L heme, the Rieske Fe_2S_2 cluster or the cyt c_1 in their paramagnetic states. In addition, the other monomer in the functional dimer has a similar range of possible redox states which may be further complicated by cooperativity or electron transfer between monomers and conformational heterogeneity of the Rieske headgroup. The same SQ_o radical can have more than 100 different states of the protein around it, each state causing a different PRE.

Most of the potential paramagnetic centers around SQ_o are too distant to cause a significant PRE on the T_M. The observed PRE is adequately fit considering only two dominant reduced hemes interacting with the SQ_o. That means there are four sets of states whose populations control the PRE and must be specified. A simplification is possible by assuming that the probabilities of either of those two hemes being in the paramagnetic, reduced state are independent of each other. The PRE fits for the best sets of experimental data found that probability to be 30%, meaning that 49% of the SQ_o has both dominant hemes oxidized and lacking PRE; 42% have one heme reduced and producing PRE; and 9% have both hemes reduced and producing PRE. The net PRE for SQ_o is the weighted sum of the individual contributions. The temperature-independent background decay of the SQ_o spin echo is multiplied by this temperature-dependent PRE, so one is, in effect, fitting the changes in the spin echo decay of SQ_o.

References.

[1] L. Esser, B. Quinn, Y. F. Li, M. Q. Zhang, M. Elberry, L. Yu, C. A. Yu, D. Xia, *J. Mol. Biol.,* **2004**, *341*, 281-302.

[2] A. T. Laurie, R. M. Jackson, *Bioinformatics,* **2005**, *21*, 1908-1916.

[3] S. R. Solmaz, C. Hunte, *J. Biol. Chem.,* **2008**, *283*, 17542-17549.

[4] a) W. Lubitz, G. Feher, *Appl. Magn. Reson.,* **1999**, *17*, 1-48; b) W. Lubitz, E. C. Abresch, R. J. Debus, R. A. Isaacson, M. Y. Okamura, G. Feher, *Biochim. Biophys. Acta,* **1985**, *808*, 464-469.

[5] R. A. Isaacson, E. C. Abresch, M. L. Paddock, G. Feher, F. Lendzian, W. Lubitz, *Biophys. J.,* **1998**, *74*, A135-A135.

[6] E. Martin, R. I. Samoilova, K. V. Narasimhulu, T. J. Lin, P. J. O'Malley, C. A. Wraight, S. A. Dikanov, *J. Am. Chem. Soc.,* **2011**, *133*, 5525-5537.

[7] A. Schnegg, A. A. Dubinskii, M. R. Fuchs, Y. A. Grishin, E. P. Kirilina, W. Lubitz, M. Plato, A. Savitsky, K. Mobius, *Appl. Magn. Reson.,* **2007**, *31*, 59-98.

[8] F. MacMillan, F. Lendzian, W. Lubitz, *Magn. Reson. Chem.,* **1995**, *33*, S81-S93.
[9] F. MacMillan, S. Kacprzak, P. Hellwig, S. Grimaldi, H. Michel, M. Kaupp, *Faraday Discuss.,* **2011**, *148*, 315.
[10] a) L. L. Yap, R. I. Samoilova, R. B. Gennis, S. A. Dikanov, *J. Biol. Chem.,* **2007**, *282*, 8777-8785; b) L. L. Yap, R. I. Samoilova, R. B. Gennis, S. A. Dikanov, *J. Biol. Chem.,* **2006**, *281*, 16879-16887.
[11] S. Grimaldi, F. MacMillan, T. Ostermann, B. Ludwig, H. Michel, T. Prisner, *Biochemistry,* **2001**, *40*, 1037-1043.
[12] M. Rohrer, F. MacMillan, T. F. Prisner, A. T. Gardiner, K. Möbius, W. Lubitz, *J. Phys. Chem. B,* **1998**, *102*, 4648-4657.
[13] a) J. A. Weil, J. R. Bolton, J. E. Wertz, *Electron paramagnetic resonance elementary theory and practical applications*, 2nd ed., Wiley-Interscience, New York, **2007**; b) G. Gescheidt, in *Electron Paramagnetic Resonance - A Practitioner's Toolkit* (Eds.: M. Brustalon, G. E.), John Wiley & Sons, Hoboken, **2009**, pp. 109-158.
[14] J. L. Cape, M. K. Bowman, D. M. Kramer, *Proc. Natl. Acad. Sci. USA,* **2007**, *104*, 7887-7892.
[15] a) M. Weger, *At&T Tech J,* **1960**, *39*, 1013-1112; b) R. S. Alger, *Electron paramagnetic resonance; techniques and applications*, Interscience Publishers, New York,, **1968**.
[16] a) K. M. Salikhov, Y. D. Tsvetkov, in *Time Domain Electron Spin Resonance* (Eds.: L. Kevan, R. N. Schwartz), John Wiley, New York, **1979**, pp. 231-278; b) K. M. Salikhov, A. G. Semenov, Y. D. Tsvetkov, *Electron Spin Echoes and Their Applications*, Nauka, Novosibirsk, **1976**; c) W. B. Mims, in *Electron Paramagnetic Resonance* (Ed.: S. Geschwind), Plenum, New York, **1972**, pp. 263-352.
[17] N. V. Surovtsev, N. V. Ivanisenko, K. Y. Kirillov, S. A. Dzuba, *J. Phys. Chem. B,* **2012**, *116*, 8139-8144.
[18] a) B. K. Rao, A. M. Tyryshkin, A. G. Roberts, M. K. Bowman, D. M. Kramer, *Biochemistry,* **2000**, *39*, 3285-3296; b) S. Lyubenova, M. K. Siddiqui, M. J. M. P. de Vries, B. Ludwig, T. F. Prisner, *J. Phys. Chem. B,* **2007**, *111*, 3839-3846; c) M. Sarewicz, M. Dutka, W. Froncisz, A. Osyczka, *Biochemistry,* **2009**, *48*, 5708-5720.